AEGC Australasian Exploration Geoscience Conference Brisbane 2021

3-D Gravity Geometry Inversion of the Matheson Area, Abitibi greenstone belt: maintaining the contacts of one of the geological unit fixed for obtaining superior results.

Fabiano Della Justina
Mineral Exploration Research Centre, Laurentian University
Sudbury, Ontario P3E 2C6, Canada
fjustina@laurentian.ca

Richard S. Smith
Mineral Exploration Research Centre, Laurentian University
Sudbury, Ontario P3E 2C6, Canada
RSSmith@laurentian.ca

SUMMARY

Using measured density values and surface geology as constraints, and a compilation of two data sets of ground gravity as observed data, 3-D inversions using the VPmg algorithm were used to estimate the subsurface model in the Matheson area, which is located in the southern part of the Abitibi greenstone belt, Canada. Besides the aforementioned constraints, the contacts of the Porcupine metasedimentary assemblage (one of the 9 geological units presented in the study area) were fixed during the inversion. This was because priori 2-D forward modelling had derived a model also consistent with reflection seismic data. When the Porcupine assemblage contacts were free to move, the thickness was judged to be geologically unrealistic. However, when the Porcupine assemblage contacts were fixed, the model was realistic and there was a smaller misfit between predicted and observed data. The criteria to judge whether a model was realistic or unrealistic was the geological likelihood of the geometries and depths of the geological units that are obtained from an inversion.

Key words: gravity, inversion, seismic, density, Abitibi.

INTRODUCTION

Gravity inversion is an important tool for interpreting and understanding geological structures in the subsurface. The main goal of an inversion is to perturb a geophysical/geological model to accomplish an acceptable level of reproducibility of the model data with the observed data (Fullagar and Pears, 2007). There are several inversion techniques described in the literature. Some of them are well established and have been used extensively in the geophysical-data-interpretation workflow; others are still developing. Regardless of which technique is utilized more realistic results are usually achieved when geological constraints are taken into account (Mahmoodi et al., 2015; Darijani et al., 2020). In this study, two different strategies were compared. In the first strategy, all of the geological unit contacts were free to move, in the second one, the contacts of one of the geological units were fixed, while the contacts of all the remained units were free to move. In both cases, the starting model and densities constraints were the same and the units mapped at surface were used as a constraint. It was possible to fix the contacts of one of the units because priori 2-D forward gravity modelling had derived a model, which was also consistent with reflection seismic data (Della Justina and Smith, 2020).

The study is located in the Matheson area, which covers the eastern extension of the Timmins-Porcupine gold camp in Ontario – Canada (*See* Figure 1-*i*), which is one of the most important gold camps hosted in an Archaean greenstone belt (Bateman et al., 2005). The Matheson study area (MSA) also lies in the larger Timmins-Kirkland Lake region of the Abitibi greenstone belt (AGB), which also contains major Cu-Zn and Ni-Cu-PGE mineralization (Monecke et al., 2017). The geology of the MSA is divided in five main lithotectonic assemblages and two main intrusions (Figure 1-*ii*). There are also two main faults, which have been associated with several deposits. The gravity modelling of Della Justina and Smith (2020) was intended to better understand the faults geometry, as this was not well resolved in the seismic data, but the modelling also helped understand other geological features, such as geological assemblages, and geological intrusions at the study area.

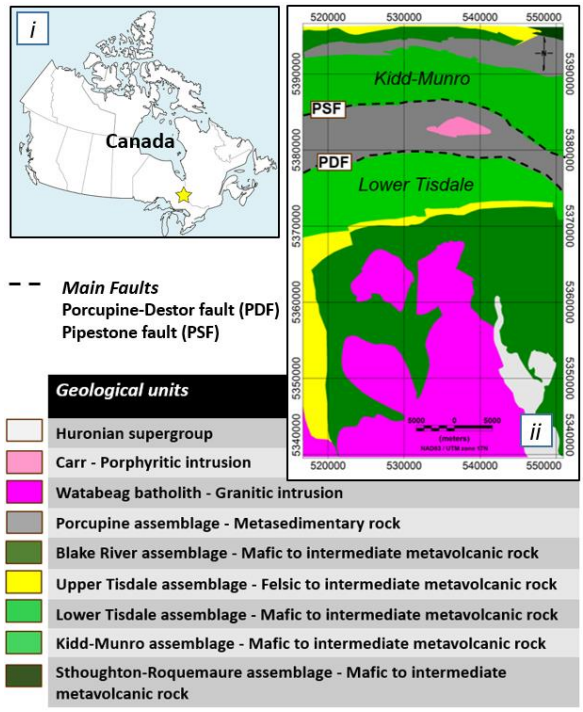

Figure 1. The study area location map on the top-left (*i*), the geological map (modified after Ayer et al., 2005) of the Matheson area on the right with the legend at the bottom (*ii*), where the 3-D modelling has been carried out.

GEOLOGY OF THE AREA

The metasedimentary Porcupine assemblage is the geological unit bounded by the two mineral endowed main faults. The Porcupine assemblage consists predominantly of wacke, siltstone and mudstone and is bordered by mafic to intermediate

metavolcanic rocks (depicted as light green on Figure 1-*ii*). To the south is the Lower Tisdale assemblage, which consists predominantly of tholeiitic mafic volcanic rocks with localized accumulations of komatiite, intermediate to felsic calc-alkaline volcanic rocks and iron formation. The rocks to the north of the Porcupine are the Kidd-Munro assemblage, which is dominated by tholeiitic mafic and komatiitic rocks with localized accumulations of tholeiitic felsic volcanic rocks (Ayer et al., 2007). The main fault to the north is the Pipestone Fault (PSF), which separates the Kidd-Munro assemblage to the north from the Porcupine assemblage to the south. The Porcupine Destor fault (PDF) demarcates the southern contact of the Porcupine assemblage with the Tisdale assemblage further to the south. Both these faults are shown on Figures 1-*ii* and 2-*i* with black dashed lines.

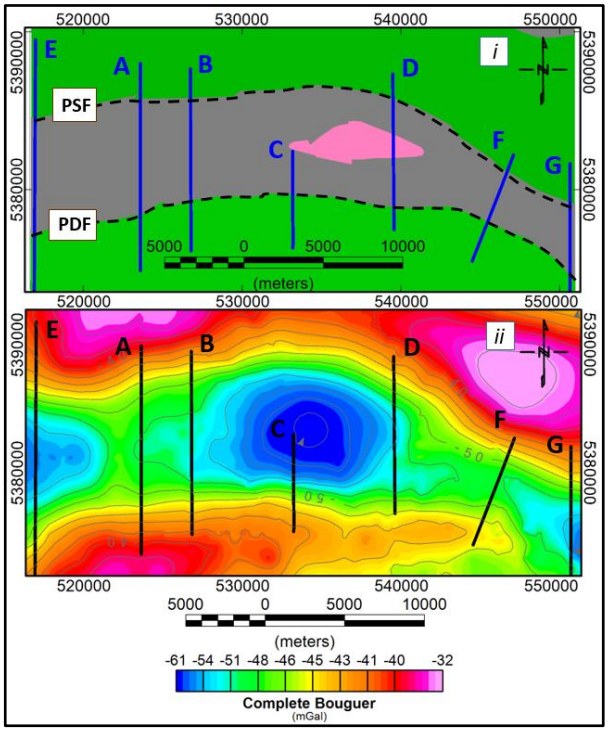

Figure 2. Complete Bouguer anomaly gravity grid in the Porcupine assemblage study area. The data was obtained for the Metal Earth project and the Geological Survey of Canada compilation.

2-D GRAVITY MODELLING

The gravity data used in the 2-D modelling has been acquired/compiled as part of the geophysical component of the Metal Earth (ME) project. The ME gravity data was acquired in the 2018 field season along traverse B, traverse C, and traverse D (Figure 2). All gravity readings of the ME data were taken using Scintrex CG-6 Autograv™ gravity meters. The positions and heights were measured with a Trimble R2 GNSS receiver and differential corrects made using Fieldpoint RTX software. GNSS refers to global navigation satellite systems, which include the GPS and GLONASS systems. Survey stations were chosen alongside roads or within walking distance from roads with an average spacing between the stations of 300 m. These stations were tied to an existing Canadian Gravity Station Network base station (Highway 101 - 9656-1970). In addition, side road measurements with distances up to 1 km from the traverses were acquired when road access permitted (Maleki et al. 2018).

Unlike the aforementioned 3 lines, the gravity data along the traverse A was obtained from the Geological Survey of Canada (GSC) gravity compilation (NRCan, 2016).

ME acquired and GSC compiled measurements were processed and corrections applied to remove unwanted variations associated with changes in latitude and elevations (Dentith and Mudge, 2014) to calculate the final "Complete Bouguer Anomaly" (Nowell, 1999). These corrections were applied using Oasis Montaj® (https://www.seequent.com/products-solutions/geosoft-oasis-montaj/). The gravity data from the Geological Survey of Canada extended well beyond the seismic line, so we could generate the gravity grid shown in Figure 2-*ii*. Uncertainties were estimated for the measurements and the data reduction steps using the error propagation equation (Bevinton et al. 2003). The final uncertainty in the complete Bouguer anomaly for Metal Earth data was 0.3 mGal. Although the gravity station spacing for traverse A (the Shillington line) was in some cases as low as 100 m, the uncertainty quantified by the data acquirer/provider was 1 mGal.

Four high-resolution seismic reflection profiles were utilized to help construct the initial model for some of the 2-D models, as these provide high resolution images of structures within the crust. The traverse A seismic line data was acquired during the Discover Abitibi Initiative and the other three (B, C, and D) were part of the Metal Earth project (Snyder et al. 2009; Naghizadeh et al. 2019). All the seismic profiles were acquired using Vibroseis sources. The Metal Earth high-resolution surveys utilized source and receiver spacing of 6.25 and 12.5 m (Cheraghi et al. 2020). The traverse A high-resolution line was recorded with 12.5 m receiver interval and 25 m shot interval (Snyder et al. 2009). The data used to constrain the construction of the models were the subcrop (surface) geology, densities (Table 1) from a database compiled as part of the Metal Earth project (Eshaghi et al. 2019) as well as an interpretation of the seismic profiles themselves.

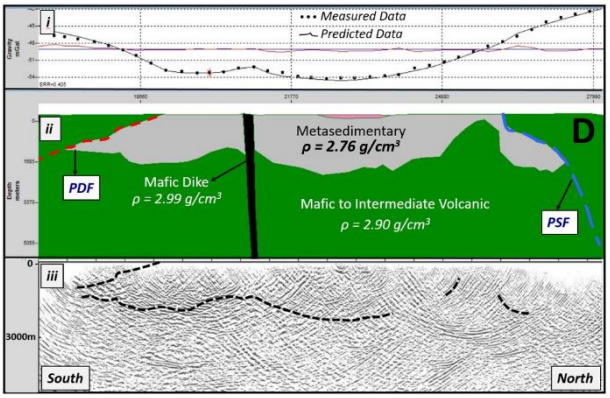

Figure 3. The traverse D modelling showing the measured and predicted gravity data and the difference (red line) (*i*), the model itself providing density parameters and faults localizations (*ii*), and the interpreted seismic section (*iii*).

Whereas seismic data are available for traverses A, B, C, and D seismic data were not available for traverses E, F and G (Figure 2). The latter three traverses were intended to extrapolate the modelled sections to the west and east and were built solely using surface geology, gravity data and data from the density compilation.

The gravity data along the profiles were modelled with the 2-D forward modelling program GM-SYS. This process involves the forward modeller manually adjusting the model parameters

until the predicted data and the measured data agree to within the uncertainty level of the data. For brevity, we are only showing the gravity data (Figure 3-*i*) and final model (Figure 3-*ii*) for section D. A high resolution seismic section (Figure 3-*iii*) was interpreted and used to help construct the initial model whenever it was available (sections A, B, C, and D).

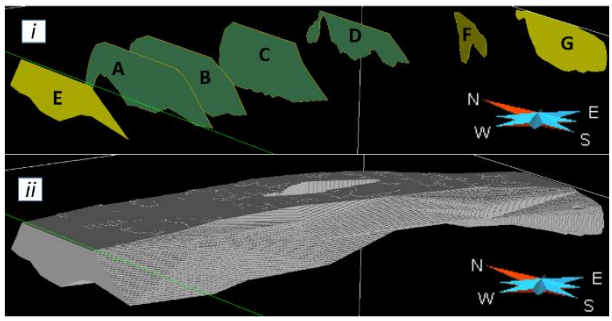

Figure 4. The modelled cross sections of the Porcupine assemblage (*i*) distinguishing between the section that the 2-D modelling could benefit of available high resolution seismic sections (darker green) and those they could not (lighter green). At the bottom (*ii*), the created 3-D surface from the cross sections (*i*).

The seven 2-D models of the geometry of the Porcupine assemblage are summarized in (Figure 4-*i*) and from these cross sections, a 3-D surface was generated (Figure 4-*ii*).

3-D GEOMETRY INVERSION

The initial 3-D density model was built in a volume 56 × 34 km horizontally and 25 km vertically. The horizontal and vertical resolution were 100 and 25 m respectively. Topographic information (Shuttle Radar Topographic Mission [SRTM] 30 m) used for this inversion was downloaded from the Geosoft public DAP server (http://dap.geosoft.com). The inversion started with an initial geometry based on the surface geology, with the thicknesses set to 1 km and the contacts as vertical (Figure 5-*i*). The exception is the Porcupine assemblage, where the initial geometry was interpolated from the 2-D modelling as described above (*see* Figures 4-*ii* and 5-*i*).

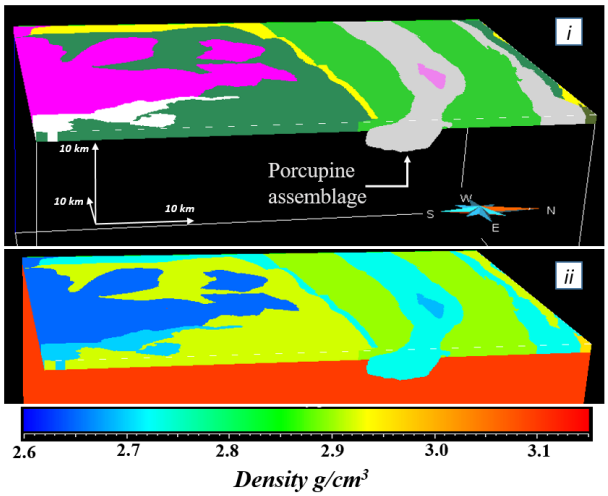

Figure 5. The starting model represented by the colours used to represent the surface geology, while in (*i*) the colours correspond to the assigned density values associated with the assemblages and intrusions (*ii*), as shown on the colour bar.

Like the 2-D modelling, the 3-D inversion used density values from a Metal Earth project compilation. The average density values were computed for each geological unit and are displayed in Table 1 and represented in Figure 5-*ii*. The density value for the region underneath the assemblages and intrusion was 3.10 g/cm^3 representing the middle crust density. The gravity data was also from a compilation of the GSC and the ME project (Figures 6-*ii* or 7-*ii)*, from which 1144 ground gravity station were selected as being in the study area. The 3-D modelling used the free-air corrected gravity data as the inversion software is able to account for changes in height and the gravitational effect of topographic variations. This differs from the 2-D modelling, which used the Bouguer anomaly data.

Geological unit	Density (g/cm^3)	Std. Dev. (g/cm^3)
Huronian supergroup	2.71	0.03
Carr	2.69	0.02
Watabeag	2.65	0.08
Porcupine	2.76	0.09
Blake River	2.91	0.16
Upper Tisdale	2.77	0.07
Lower Tisdale	2.86	0.11
Kidd-Munro	2.90	0.13
Sthoughton-Roquemaure	2.99	0.08

Table 1. Densities averages for the assemblages and intrusions in the Matheson 2-D and 3-D modelling areas. Data has been compiled as part of the Metal Earth project.

In a geometry inversion of gravity data, the density values are not allowed to change, just the geometries of the assigned units are modified to fit the observed data. As well, constraints might be added, i.e., surface geology, drilling information, etc. In this study the surface geology was used as a constraint, which implies that the unit contacts are free to move, except on the surface. The VPmg version 9.0 (Fullagar and Pears, 2007) linked to the Mira Geoscience GOCAD mining suite was used to perform the inversions.

The main goal of this study is comparing two different inversion approaches. In the first approach, all the contacts are unconstrained geometrically and free to move up or down, while in the second approach, the depths to the base of the Porcupine assemblage, were fixed. In both approaches, the internal contacts of the Porcupine assemblage, which separates it from the Carr intrusion, were still free to move. The reason why this internal contact was not fixed, was because it was not well resolved at the forward modelling stage, mostly due to difficulties in identifying the boundaries in the seismic data.

In the first approach (all the contacts are free to vary in depth), the smallest misfit was obtained after 91 iterations, returning a root mean square (RMS) misfit of 9.34 mGal from an initial value of 34.03 mGal. The final results for this inversion are shown in Figure 6.

The second inversion, where the external contacts of the Porcupine were fixed, as well as the surface contacts of all units, returned the best RMS misfit after 60 iterations. The final achieved misfit for this inversion was 2.31 mGal and the results are shown in Figure 7.

DISCUSSION AND CONCLUSIONS

The inversion where the geometry of the Porcupine assemblage is fixed has a smaller final misfit (2.31 mGal) than the case when all of the contacts were free to move (9.34 mGal). This smaller residual data (Figure 6-*iv* in comparison to Figure 7-*iv*) indicates that the Porcupine fixed-geometry case better explains the gravity data. As well, in the case of the unconstrained-geometry inversion the thicknesses of all the units in Figure 7-*i* Figure 6-*i* are too thick compared with the results of Snyder et al. (2008) and Haugaard et al (2021).

The gravity forward modelling, which was conducted to determine the geometry of the Porcupine assemblage in part of the study area, took a considerable amount of time and effort; the results were very beneficial in obtaining a more reasonable inverse model of the entire study area. Those extra constraints, added during the inversion by fixing the contacts of the Porcupine assemblage, made the inversion more stable, required less iterations and provided a smaller misfit. The forward modelling benefited significantly from seismic sections available in the area, which helped to construct and constrain the 2-D models. The seismic data in the area was difficult to interpret, but fortunately, there was an identifiable interface that could reasonably be interpreted as the base of the Porcupine assemblage, so this contact was fixed during the inversion. Therefore, whenever seismic sections are available, the interfaces which can be interpreted should be taken into account when building the model, Whether or not these interfaces are allowed to vary in subsequent modelling will depend on the quality of the data, the confidence with which they are interpreted and the objective of the modelling exercise. In our case, we found that allowing them to vary was not beneficial.

In what we report here, fixing the contacts of one unit has provided superior results, but it should be pointed out that the final misfit could still be reduced to values closer to the data uncertainty, which was 1 mGal for the majority of the gravity stations. This could be done perhaps by including more geological units, such as smaller intrusions. Another approach might be to have smaller cell sizes. However, this extra complexity on the model would require more finely sampled gravity data to constrain the model at locations that are currently not well sampled. Other factors, which might have contributed to not having a smaller misfit, are all the inherent assumptions that were used in the 2-D modelling, such as the infinite strike length of units. The 3-D modelling should be able to overcome this weakness, by allowing variable strike lengths, but this was not the case for some unclear reason. Another possible flaw in our procedure is that when the 3-D surfaces are created by interpolation from the cross sections, we could have added in biases due to the fact that the resulting geometry was too simple.

ACKNOWLEDGEMENTS

This research has been funded by the Canada First Research Excellence Fund. The authors would like to thank the Metal Earth project at Laurentian University for providing gravity, seismic and petrophysical data. They also would like to thank Seequent, Mira Geoscience Ltd., and Emerson paradigm for providing specialized software. This is Metal Earth publication MERC-ME-2021-38.

REFERENCES

Ayer, J.A., Thurston, P.C., Bateman, R., Dubé, B., Gibson, H.L., Hamilton, M.A., Hathway, B., Hocker, S.M., Houlé, M.G., Hudak, G., Ispolatov, V.O., Lafrance, B., Lesher, C.M., MacDonald, P.J., Péloquin, A.S., Piercey, S.J., Reed, L.E. and Thompson, P.H., 2005, Overview of results from the Greenstone Architecture Project: Discover Abitibi Initiative; Ontario Geological Survey, Open File Report 6154.

Ayer, J. A., B. Dubé, and P. Ross, 2007, The Abitibi Greenstone Belt : Update of the Precambrian Geoscience Section Program , the Targeted Geoscience Initiative III Abitibi and Deep Search Projects: Ontario Geological Survey, Open File Report 6213.

Bateman, R., J. A. Ayer, B. Dubé, and M. A. Hamilton, n.d.The Timmins-Porcupine Gold Camp, Northern Ontario: The Anatomy of an Archaean Greenstone Belt and Its Gold Mineralization: Discover Abitibi Initiative: Ontario Geological Survey, Open File Report 6158.

Bevington, P. R., and D. K. Robinson, 2003, Data reduction and error analysis for the physical sciences: McGraw-Hill Higher Education.

Cheraghi, S., M. Naghizadeh, D. Snyder, R. Haugaard, and T. Gemmell, 2020, High-resolution seismic imaging of crooked two-dimensional profiles in Greenstone Belts of the Canadian Shield: Results from the Swayze Area, Ontario, Canada: Geophysical Prospecting, 68,62–81.

Darijani, M., C. G. Farquharson, and P. G. Lelièvre, 2020, Clustering and constrained inversion of seismic refraction and gravity data for overburden stripping: Application to uranium exploration in the Athabasca Basin, Canada: Geophysics, 85, B133–B146.

Della Justina, F., and R. Smith, 2020, 2D forward gravity and magnetic modeling of the Porcupine assemblage, Matheson area: SEG International Exposition and 90th Annual Meeting, Expanded Abstracts, 999–1003.

Dentith, M., and S. T. Mudge, 2014, Geophysics for the mineral exploration geoscientist: Cambridge University Press.

Eshaghi, E., R. S. Smith, J. Ayer, 2019, Petrophysical characterisation (i.e. density and magnetic susceptibility) of major rock units within the Abitibi Greenstone Belt: Laurentian University Mineral Exploration Research Centre, publication number MERC-ME-2019-144. https://merc.laurentian.ca/research/metal-earth/reports Accessed March 26, 2021.

Fullagar, P., and G. Pears, 2007, Towards geologically realistic inversion: in B. Milkereit, Proceedings of Exploration 07: Fifth Decennial International Conference on Mineral Exploration. 444–460.

Haugaard, R., F. Della Justina, E. Roots, S. Cheraghi, R. Vayavur, G. Hill, D. Snyder, J. Ayer, M. Naghizadeh, and R. Smith, 2021, Crustal-Scale Geology and Fault Geometry Along the Gold-Endowed Matheson Transect of the Abitibi Greenstone Belt: Economic Geology: 116(5) 1053-1072. doi: 10.5382/econgeo.4813

Maleki, A., W. J. McNeice, F. Justina, E. Eshaghi, and R. S. Smith, 2018, Potential field data acquisition and compilation across metal earth's areas of interest: Summary of Field Work and Other Activities, 2018, Ontario Geological Survey, Open-File Report 6350, p.46-1 to 46-5.

Mahmoodi, O., R. S. Smith, and B. Spicer, 2017, Using constrained inversion of gravity and magnetic field to produce a 3D litho-prediction model: Geophysical Prospecting, 65, 1662–1679.

Monecke, T., P. Mercier-Langevin, and B. Dubé, 2017, Archean Base and Precious Metal Deposits, Southern Abitibi Greenstone Belt, Canada: Archean Base and Precious Metal Deposits, Southern Abitibi Greenstone Belt, Canada, 19.

Nowell, D. A. G., 1999, Gravity terrain corrections —an overview: Journal of Applied Geophysics, 42, 117–134.

Naghizadeh, M., D. Snyder, S. Cheraghi, S. Foster, S. Cilensek, E. Floreani, and J. Mackie, 2019, Acquisition and processing of wider bandwidth seismic data in crystalline crust: Progress with the metal earth project: Minerals, 9, 145.

NRCan (Natural Resources Canada), 2016, Geoscience data repository for geophysical data, http://gdr.agg.nrcan.gc.ca/gdrdap/dap/search-eng.php, Accessed March 26, 2021.

Snyder, D. B., W. Bleeker, L. E. Reed, J. A. Ayer, M. G. Houle, and R. Bateman, 2008, Tectonic and Metallogenic Implications of Regional Seismic Profiles in the Timmins Mining Camp: Economic Geology, 103. 1135–1150.

Snyder, D. B., P. Cary, and M. Salisbury, 2009, 2D-3C High-Resolution Seismic Data from the Abitibi Greenstone Belt, Canada: Tectonophysics, 472, 226–237.

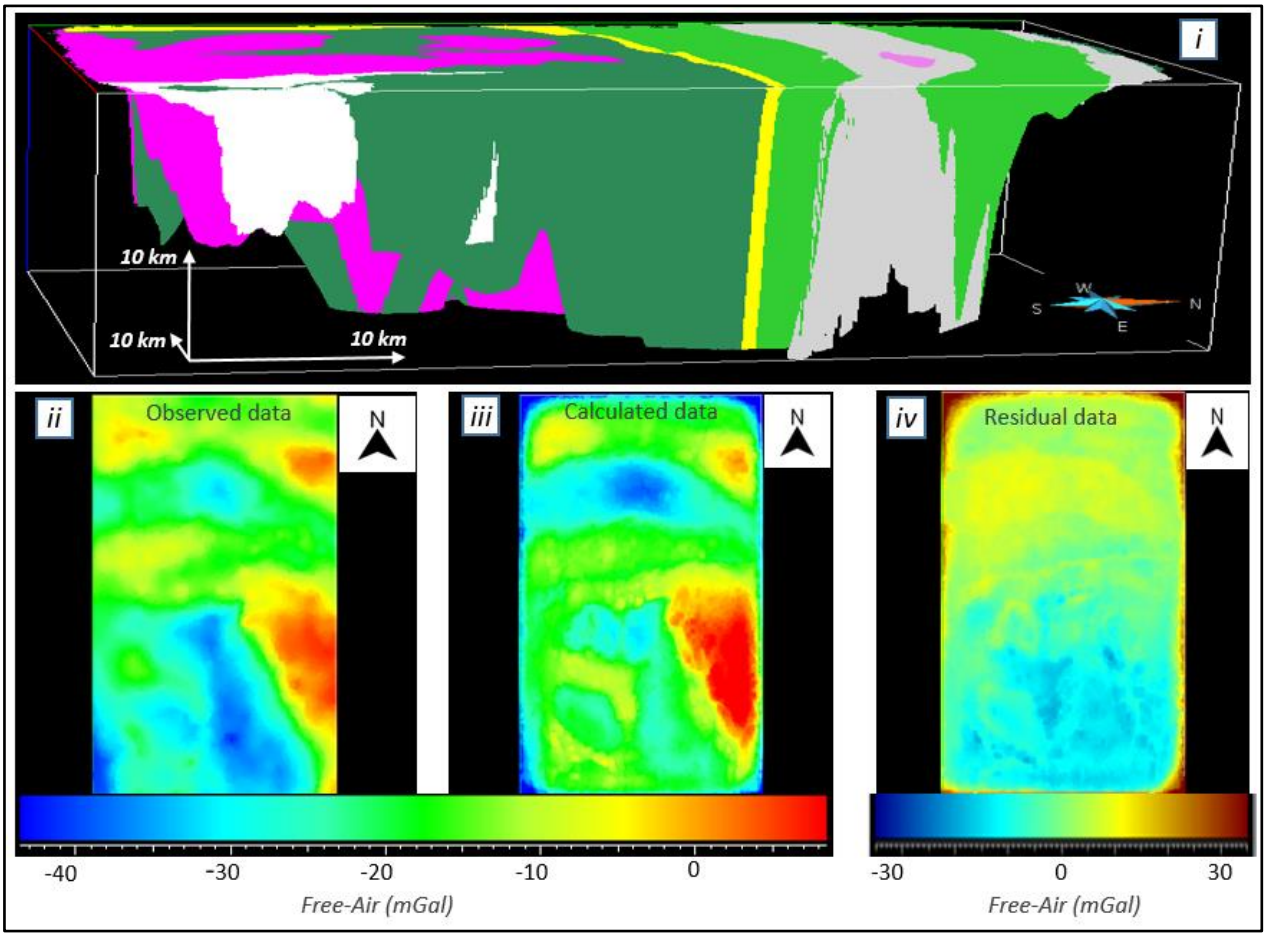

Figure 6. Final inverse model (*i*) in the case when the Porcupine assemblage contacts in depth were free to move. The calculated data for this model is shown in the grid in (*iii*). The differences between the observed – Free-Air anomaly grid - (*ii*) and calculated grids are shown as the residual grid (*iv*).

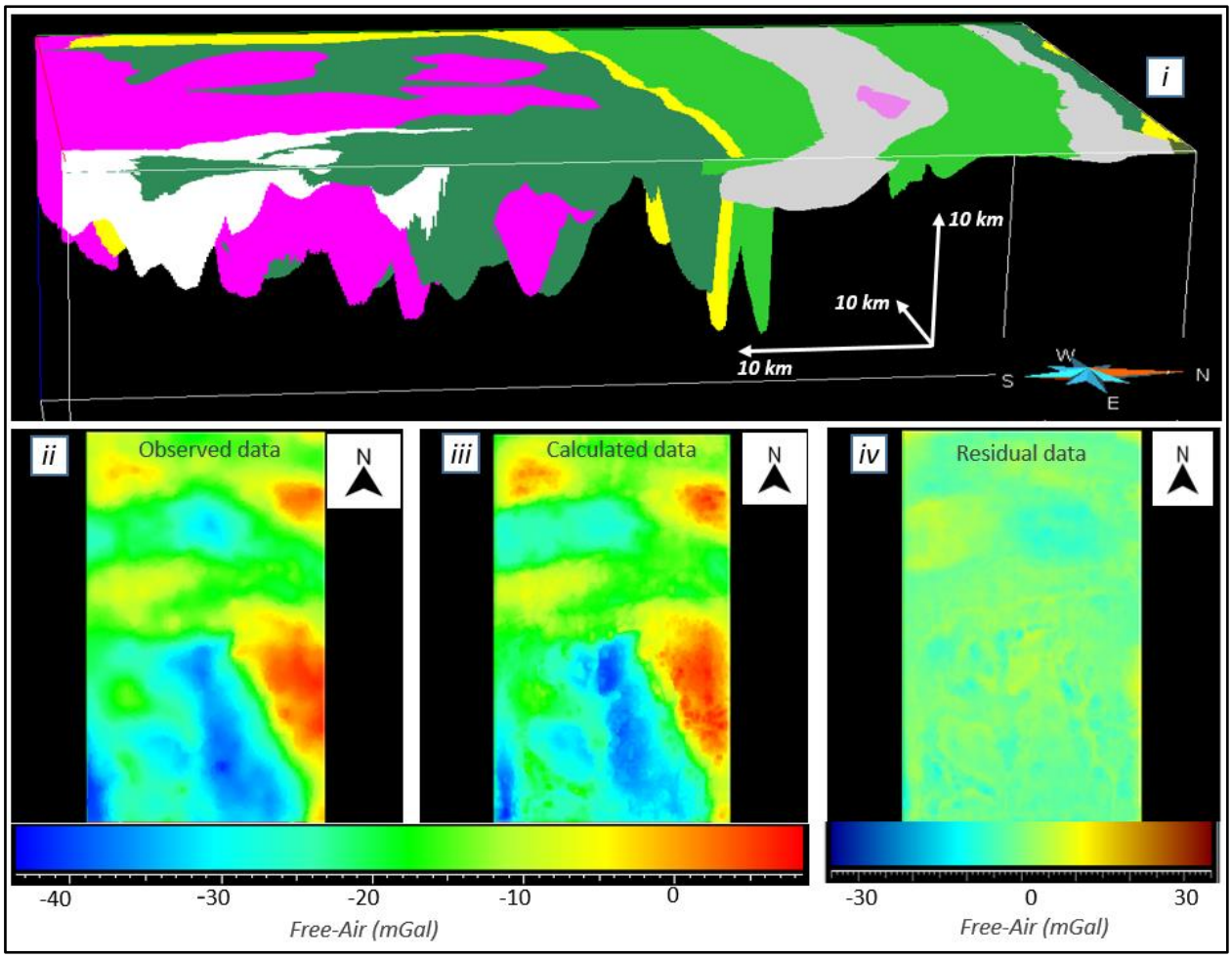

Figure 7. Final inverse model (*i*) in the case when the Porcupine assemblage contacts are fixed in depth. The calculated data for this model are shown in the grid in (*iii*). The differences between the observed – Free-Air anomaly grid - (*ii*) and calculated grids are shown as the residual grid (*iv*).